

BIOREMEDIATION SCIENCE AND TECHNOLOGY RESEARCH

BSTR VOL 11 NO 2 2023

Website: http://journal.hibiscuspublisher.com/index.php/BSTR/index

A Fixed-Bed Study on the Feedsorption of BSA Using PKC: Toward the Sustainable Agrisorption of Protein-rich Waste for Enhancing Low Nutritional-value Feed

Mohd Ezuan Khayat^{1,2} and Mohd Yunus Shukor^{1,2}*

¹Department of Biochemistry, Faculty of Biotechnology and Biomolecular Sciences, Universiti Putra Malaysia, UPM 43400 Serdang, Selangor, Malaysia.

²Agribiotechnology Group, Faculty of Biotechnology and Biomolecular Sciences, Universiti Putra Malaysia, UPM 43400 Serdang, Selangor, Malaysia.

Email: mohdyunus@upm.edu.my

HISTORY

Received: 25th Oct 2023 Received in revised form: 15th Dec 2023 Accepted: 29th Dec 2023

KEYWORDS

Biosorption Agrisorption Feedsorption PKC

ABSTRACT

Palm Kernel Cake (PKC), a by-product of Malaysia's palm oil industry, stands out as a sustainable and cost-efficient feed ingredient. However, its use is nutritionally limited for monogastric animals due to high fiber content and anti-nutritional factors. This groundbreaking study explores the innovative process of 'feedsorption'—a term we have coined under the broader concept of 'agrisorption'—to enhance the nutritional value of PKC. By adsorbing protein-rich agricultural, poultry, and farm animal wastes, represented by bovine serum albumin (BSA), we aim to elevate PKC's protein content. Through detailed experimentation involving varying bed depths (1 cm to 2 cm) and initial BSA concentrations (100 to 500 μg/mL) within fixed-bed columns, our findings reveal that increased bed depths significantly prolong breakthrough and exhaustion times, highlighting improved adsorption efficiency. Yet, depths beyond 1 cm pose a risk of clogging. Higher BSA concentrations were found to accelerate breakthrough, indicating a stronger driving force capable of overcoming mass transfer resistance. The Modified Dose Response (MDR) model outperformed the Thomas model in accurately predicting breakthrough curves across different conditions. This study not only confirms the feasibility of feedsorption to bolster the nutritional profile of low-quality feed using protein-rich waste but also introduces a promising avenue for enhancing sustainable livestock nutrition.

INTRODUCTION

The oil palm industry, particularly in Malaysia, has seen PKC emerge as a significant by-product used in animal feed, reflecting broader trends towards sustainability and cost-efficiency in livestock production. The anticipated 21% increase in livestock production between 2010 and 2025 underscores the pressing need for sustainable feedstock solutions. This growth translates into a projected increase in global feed demand from 6.0 to 7.3 billion tonnes of dry matter, highlighting the critical role of innovative feed ingredients like PKC in meeting this surge (Kim et al., 2019). Malaysia, a leading player in the oil palm sector, has consistently produced approximately 1.3 million metric tonnes of PKC annually since 1996. This figure saw a significant rise to 2.4 million metric tonnes by 2022, as reported by the Malaysian Palm Oil Board. The export markets for Malaysian PKC are diverse, with significant shipments to Japan, Singapore, and Europe.

Europe, in particular, has shown a keen interest in PKC for its sustainable and cost-effective properties as an animal feed ingredient. The price of PKC has fluctuated over the years, influenced by global oil prices, demand for palm oil products, and the overall supply of PKC. For instance, PKC prices have ranged from \$200 to \$300 per metric tonne, varying with market conditions and production levels. PKC offers a cost-effective alternative to traditional feedstocks, partly due to its by-product status and the efficiency of palm oil production. Its use can significantly reduce feed costs for livestock farmers, contributing to more sustainable farming practices.

The utilization of PKC in animal feed contributes to the circular economy model by maximizing the value extracted from oil palm cultivation. This approach not only reduces waste but also lessens the environmental footprint of both the palm oil and livestock industries. Despite its high fiber and moderate protein

content, which limits its use for monogastric animals, PKC has been successfully incorporated into ruminant diets. Research and technological advancements are ongoing to enhance its nutritional profile for broader applications.

The increase in PKC production to 2.4 million metric tonnes in 2022, coupled with its price range, suggests a significant revenue stream for Malaysia's palm oil sector. Assuming an average price of \$250 per metric tonne, the PKC market could represent a gross annual revenue of approximately \$600 million, underscoring its economic importance. In Malaysia alone, the export for 2021 was alone worth RM1.5 billion [1]. The global shift towards sustainable and environmentally friendly products has bolstered the demand for PKC. As countries and industries strive to reduce their carbon footprint, PKC's role in animal nutrition is poised for growth, reflecting broader trends in sustainability and resource efficiency. PKC stands at the intersection of environmental sustainability and economic viability, offering a promising solution to the growing demand for livestock feed. Its production and export from Malaysia to countries like Japan, Singapore, and Europe highlight its global significance, while ongoing research aims to unlock its full potential as a sustainable feedstock.

Palm Kernel Cake (PKC), a by-product of palm oil production, is recognized for its application in livestock feed, yet its nutritional efficacy, particularly the bioavailable protein content, is subject to critical evaluation. The protein content in PKC varies from 14% to 22%, but its utilization by animals, especially monogastrics like poultry and pigs, is limited due to high fiber content and the presence of anti-nutritional factors (ANFs) such as tannins and phytates. These elements not only restrict the digestibility of proteins but also their absorption, thereby impacting the overall nutritional value of PKC. Furthermore, the amino acid composition of PKC might not align with the specific dietary requirements of certain livestock, necessitating additional nutritional supplementation to ensure a balanced diet. To enhance the bioavailability of proteins in PKC, various processing methods and dietary strategies are being explored.

Techniques such as mechanical and chemical processing aim to reduce fiber content and deactivate ANFs, thereby improving nutrient digestibility. Additionally, the inclusion of enzyme supplements in PKC-based diets can further aid in breaking down fibers and ANFs, enhancing the feed's nutritional uptake. Complementing PKC with other protein sources or specific amino acids can also help in meeting the comprehensive nutritional needs of livestock. As research continues to evolve in this domain, optimizing the processing and formulation of PKC is key to unlocking its potential as a sustainable and cost-effective feed ingredient, contributing to the global efforts in sustainable livestock production.

There is an urgent call for an upgrade in the nutritional quality of PKC. In this study, we reply to the call by improving the protein content in PKC using a surrogate protein compound Bovine Serum Albumin (BSA) from agricultural waste effluents such as Palm Mill Oil Effluent or other agricultural and dairy industries and even abattoirs. We coin this process 'feedsorption', which falls under the bigger umbrella of 'agri-or agrosorption', also a new term we coin. The oil palm sector is the major industry in Malaysia, about 1.3 million metric tonnes of PKC have been produced annually since 1996. Most of the PKC produced is exported to various countries, such as Japan, Singapore, and specifically Europe, for use as an ingredient in animal feed formulations. In addition, the Malaysian Palm Oil

Board reported 2.4 million metric tonnes of PKC produced in 2022 (Malaysian Palm Oil Board, 2022). PKC is abundantly produced alongside palm kernel oil from the crushing of palm kernels, giving a yield of about 50% PKC. However, its application as a dietary source for monogastric animals is significantly restricted because of its elevated fiber and moderate protein content (Mohd Firdaus et al., 2022).

MATERIALS AND METHODS

Preparation of adsorbent and adsorbate

PKĈ was bought from a local company (Feed Enterprise). BSA was purchased from Sigma-Aldrich. All the chemicals utilised in this research were of analytical grade and every technical equipment was appropriately calibrated prior to the experiment.

Preparation of palm kernel cake

PKC was sieved to 1.25 mm using a Sieve standard for sieve size Ø200 mm, ASTM Tolerance 1.14 – 1.22 mm prior to treatment. The collected PKC were immersed in distilled water and kept overnight in the chiller prior to each experiment. Under this condition, the swelled-up size of PKC was approximate 2 mm.

Lab scale packed bed column experiments

PKC in 1 cm bed height in a glass chromatography column (XK 50/30 Cytiva, USA) column. The column is water-jacketed and has a dimension of 200 mm height and 16 mm diameter. The columns were packed into a bed height of 1, 1.5 and 2 cm bed heights. The column was preconditioned by running several hundred milliliters of 10 mM citrate buffer pH 4.8. The effect of pH was studied by ranging the pH of the buffer from 3.5 to 5.5 using 10 mM citrate buffer, $C\theta$ of 100 μ g mL⁻¹ BSA and Q of 1.5 mL/min (flow rate).

Solutions containing the adsorbate at various concentrations (ranging from 100 to 500 mg/L) were introduced into the columns using a downward flow technique, with flow rates set at 1.5 and 2 mL/min, facilitated by a Gilson peristaltic pump. Throughout these procedures, the experiments were conducted under conditions of neutral pH and ambient temperature. At one-hour intervals, effluent samples were collected to determine the times of breakthrough and exhaustion. The point of breakthrough (t_b) was identified when the concentration of the adsorbate in the effluent reached 10% of its initial value, while the exhaust time (t_e) was noted when this concentration rose to 80% of the original adsorbate concentration in the influent [2].

Column operation parameters

Creating a graph with the ratio of C_t/C_0 (the concentration of adsorbate in the effluent relative to the influent) against time (t) generates the breakthrough curves, which are defined by the area beneath these curves. The cumulative amount of adsorbate captured by the column is denoted as q_{total} and t_s refers to the stoichiometric time observed in an asymmetrical breakthrough curve [3]:

$$q_{total} = Q \int_{t=0}^{t=t_e} C_r dt$$
 (Eqn. 1)

$$t_s = \frac{1}{C_0} \int_{t=0}^{t=t_e} C_r dt$$
 (Eqn. 2)

The followings are equations utilized to model column parameters and characteristics where m represents the weight of the adsorbent (g), the equilibrium column adsorbate uptake capacity of the column is q_{eq} , R is the percentage removal of adsorbate, D_{total} is the total amount of adsorbate entering the column, U_r is the adsorbent usage rate, EBCT represents empty

bed contact time, t_u is the time of usable capacity, LUB is the length of unused column bed while L_b represents the bed column length until the breakthrough time. The volumetric flow rate (L h⁻¹) is Q and the adsorbate removal (mg L⁻¹) concentration is represented as $C_r = (C_0 - C_t)$, is , t_t is the total time (h), exhaustion time (h) is t_e and for a breakthrough curve which is symmetrical, t_s is the time at which $C_t/C_0 = 0.5$. The mass transfer zone is MTZ while t_z is the time needed for the mass transfer zone to move the column in the length of its own height and U_z is the rate of movement of mass transfer zone [3,4]:

$$q_{eq} = \frac{q_{total}}{m}$$
 (Eqn. 3)

$$P_{total} = \frac{c_0 Q t_e}{1000}$$
 (Eqn. 4)

$$R(\%) = \frac{Q_{total}}{P_{total}} \times 100$$
 (Eqn. 5)

$$MTZ = L\left(\frac{t_{e-}t_{b}}{t_{e}}\right)$$
 (Eqn. 6)

$$t_z = \frac{V_{e-}V_b}{Q}$$
 (Eqn. 7)

$$U_z = \frac{MTZ}{t_z}$$
 (Eqn. 8)

$$EBCT = \frac{V}{Q}$$
 (Eqn. 9)

$$U_r = \frac{m}{V_b} \tag{Eqn. 10}$$

$$t_u = \int_{t=0}^{t=t_b} \left(1 - \frac{c_t}{c_0}\right) dt$$
 (Eqn. 11)

$$L_b = \frac{t_u}{t_t} L \tag{Eqn. 12}$$

$$LUB = L\left(\frac{t_{s-}t_{b}}{t_{s}}\right)$$
 (Eqn. 13)

where m is the weight of the adsorbent in the column (g), MTZ is the length of the adsorption zone in the column (cm), that specifies the efficiency in the use of adsorbents in the column, L is the length of the adsorbent in the column (cm), t_b is breakthrough time (h), $V_e = Ot_e$, volume of solution treated at exhaustion (L), $V_b = Qt_b$, volume of solution treated at breakthrough (L), U_z stands for the rate at which MTZ moves up/down through the adsorbent bed (cm h⁻¹), EBCT denotes the time of contact between the water phase and the adsorbent which basically measures the critical depth and contact time for an adsorbent bed (h), U_r defined as the weight of adsorbent saturated per unit volume of adsorbate solution treated (g L^{-1}), t_u is the time at which the effluent concentration reaches its maximum permissible limit (h), L_b is the length of the bed used up to breakthrough (cm) and LUB is the length of the MTZ which remains unutilized even after the appearance of the exhaustion time (cm).

In this context, m represents the mass of the adsorbent contained within the column, measured in grams (g), while MTZ refers to the length of the adsorption zone within the column, measured in centimeters (cm). This length indicates how efficiently the adsorbent is being utilized within the column. L denotes the total length of the adsorbent bed in the column, also in centimeters. The breakthrough time, t_b , is recorded in hours (h) and marks the initial detection of adsorbate in the column effluent. The volume of the solution processed by the column at the point of exhaustion, V_e , is calculated as $V_e = Qt_e$, with Q being the flow rate and t_e the exhaustion time, resulting in a volume measured in liters (L). Similarly, the volume at breakthrough, $V_b = Qt_b$. U_z signifies the rate at which the mass transfer zone (MTZ) advances through or retreats from the adsorbent bed, given in centimeters per hour (cm/h).

The Empty Bed Contact Time (EBCT) is the duration of interaction between the water phase and the adsorbent, essentially gauging the necessary contact time and depth for the adsorption process, noted in hours (h). U_r , the usage rate of the adsorbent, is quantified as the mass of adsorbent that becomes saturated per unit volume of treated adsorbate solution, with units of grams per liter (g/L). The time t_u indicates when the effluent concentration hits its highest acceptable level, in hours (h), while L_b is the length of the adsorbent bed utilized up to the point of breakthrough, in centimeters (cm). LUB represents the portion of the MTZ that remains unused even after reaching the exhaustion time, also in centimeters.

Kinetic modelling of column adsorption data

Many kinetics models have been developed so far for predicting the breakthrough curves of adsorption process in continuous mode of operation. In this study, to analyze the dynamic behaviour of adsorbate adsorption onto the packed-column adsorbent, a few frequently used models including Thomas, Clark, MDR and BDST models were applied to the experimental data. Apart from describing the breakthrough curves more accurately, these models are useful in providing important system parameters that can be utilized to scale up packed bed column adsorption processes.

The Thomas model

This model, among the most frequently utilized in mathematical modeling of adsorption processes, operates under the premise that the kinetics of the rate-driving force adhere to second-order reversible reaction dynamics, conforming to the Langmuir adsorption-desorption isotherm, without any axial dispersion present. It is optimally employed for determining the maximal adsorption capacity of an adsorbent within column studies. It's important to note that the Thomas and Yoon-Nelson models are not recommended for use in conjunction with the Bohart-Adams model. This is due to their underlying principles being similar to a simplified version of the Bohart-Adams model, rendering them essentially interchangeable in their application. Consequently, the key parameters of the Thomas and Yoon-Nelson models (such as k_T , q_0 , k_{YN} , and τ) can be directly derived from the parameters (k_{BA} and N_0) specified by the Bohart-Adams model, facilitating a streamlined approach to analyzing adsorption dynamics within columnar systems [5,6]. A simpler mathematical expression of the same is as follows:

$$\frac{C_t}{C_0} = \frac{1}{1 + exp(A - Bt)}$$
 (Eqn. 14)

$$A = \frac{K_{Th}q_{Th}m}{Q}$$
 (Eqn. 15)

$$B = K_{Th}C_0 (Eqn. 16)$$

where A and B are the constants of the Thomas model, and t is the flow time (h). K_{Th} is the Thomas rate constant (L h^{-1} mg⁻¹), q_{Th} is the maximum solid phase concentration of the solute (mg g⁻¹), m is the mass of the adsorbent (g), Q is the flow rate (L h⁻¹) and C_{θ} is inlet adsorbate concentration $(mg L^{-1})$. A and B values can be found out by nonlinear regression analysis and subsequently, $K\tau_h$ and $a\tau_h$ can be calculated from A and B as per above mentioned correlation.

The Modified Dose Response model

The simplified numerical model as proposed by Yan et al. (2001) basically helps in minimizing the error resulting from the use of the Thomas model, predominantly at lower or higher periods of the breakthrough curve. The mathematical expression of the model is represented as below:

$$\frac{c_t}{c_0} = 1 - \frac{1}{1 + \left(\frac{V_t}{h}\right)^a}$$
 (Eqn. 17)

where a and b are MDR model constants. From the value of b. the value of the maximum solid phase concentration of the solute (q_m) can be anticipated by using the following equation:

$$q_m = \frac{bC_0}{m} \tag{Eqn. 18}$$

Statistical error functions

To assess whether there's a significant variance in model performance across those with differing numbers of parameters, statistical measures such as the adjusted coefficient of determination (adjR²), Root-Mean-Square Error (RMSE), corrected Akaike Information Criterion (AICc), Hannan-Quinn Information Criterion (HQC), Bayesian Information Criterion (BIC), bias factor (BF), and accuracy factor (AF) were employed on the same experimental dataset.

The RMSE, specifically designed to incorporate a penalty for the inclusion of additional parameters, was determined using the following equation (Eqn 19), where n represents the count of experimental observations, p denotes the number of model parameters, O_{bi} refers to the observed experimental values, and P_{di} signifies the predictions made by the model [7].

$$RMSE = \sqrt{\frac{\sum_{i=1}^{n} (Pd_i - Ob_i)^2}{n-p}}$$
 (Eqn. 19)

Bias Factor (BF) and the Accuracy Factor (AF). Ideally, for a perfect match between predicted and observed values, the Bias Factor should be precisely 1, indicating a one-to-one correlation. When the Bias Factor, as defined in Equation 2, exceeds 1, the model is considered fail-safe, suggesting it predicts values higher than the observed ones. Conversely, a Bias Factor less than 1 characterizes a fail-negative model, indicating predictions that tend to be lower than actual measurements. Furthermore, the Accuracy Factor plays a crucial role in assessing the overall precision of the model's predictions.

An Accuracy Factor lower than 1 is indicative of a model whose predictions generally fall short in accuracy. Expanding on this, the Accuracy Factor serves as a gauge for the predictive model's capacity to closely estimate real-world outcomes, with values deviating from 1 reflecting discrepancies between predicted and observed data. This evaluation framework, encompassing both the Bias and Accuracy Factors, provides a

comprehensive method for scrutinizing the validity and performance of various predictive models, thereby ensuring their effectiveness in accurately mirroring observed phenomena (Eqns. 20 and 21).

Bias factor =
$$10\left(\sum_{i=1}^{n} log \frac{(Pd_i/Ob_i)}{n}\right)$$
 (Eqn. 20)

$$Accuracy\ factor = 10 \left(\sum_{i=1}^n log \frac{|(Pd_i/Ob_i)|}{n} \right) \quad \ (\text{Eqn.}\ 21)$$

In the context of linear regression, the goodness of fit for a model is commonly assessed using the coefficient of determination, R², which quantifies the proportion of variance in the dependent variable that is predictable from the independent variable(s). However, when dealing with nonlinear regression, R² falls short in providing a meaningful comparative analysis across models, especially when there is a variance in the number of parameters between the models being compared. This limitation arises because R2 does not account for the complexity added by increasing the number of parameters, which can lead to an overfitting of the model to the data.

To address this issue and accurately evaluate the quality of nonlinear models, the adjusted R² metric is employed. Adjusted R² compensates for the model complexity by incorporating the number of predictors used, thereby providing a more reliable measure of model quality that penalizes excessive parameters that do not significantly improve model performance. This adjustment allows for a more equitable comparison between models with differing numbers of parameters, facilitating the identification of the model that best balances fit and complexity. In the adjusted R² formula, S_{ν}^2 is the total variance of the yvariable and RMS is Residual Mean Square (Eqns. 22 and 23).

Adjusted
$$(R^2) = 1 - \frac{RMS}{S_c^2}$$
 (Eqn. 22)

Adjusted
$$(R^2) = 1 - \frac{RMS}{S_Y^2}$$
 (Eqn. 22)
Adjusted $(R^2) = 1 - \frac{(1-R^2)(n-1)}{(n-p-1)}$ (Eqn. 23)

For assessing the suitability of different statistical models based on a specific set of experimental data, the Akaike Information Criterion (AIC) serves as a valuable tool. The AIC helps in comparing models by balancing the complexity of the model against how well it fits the data, thereby guiding the selection of a model that adequately describes the observed data without overfitting. However, when dealing with data sets characterized by a relatively high number of parameters compared to the number of data points, or in cases where the data points themselves are limited, the corrected Akaike Information Criterion (AICc) becomes particularly important. The AICc adjusts the AIC value to account for the sample size and the number of estimated parameters, providing a more accurate measure for model selection under these conditions. This correction is crucial for preventing the overestimation of the model's quality, ensuring a more reliable comparison and selection of models in scenarios with complex models or sparse data [8]. The AICc was calculated based on the following Eqn.

$$AICc = 2p + n1n\left(\frac{RSS}{n}\right) + 2(p+1) + \frac{2(p+1)(p+2)}{n-p-2}$$
 (Eqn. 24)

The Bayesian Information Criterion (BIC) represents another method grounded in information theory for statistical evaluation. Compared to the Akaike Information Criterion (AIC), BIC imposes a more stringent penalty on models in terms of the number of parameters they incorporate. This characteristic of BIC makes it particularly useful in situations where overfitting is a concern, as it discourages the selection of overly complex models that might fit the training data well but perform poorly on unseen data. By factoring in the number of parameters more heavily, BIC helps in identifying models that not only fit the data well but also maintain simplicity, potentially leading to better generalization in predictive applications [9].

$$BIC = n. \ln \frac{RSS}{n} + p. \ln (n)$$
 (Eqn. 25)

The Hannan-Quinn Information Criterion (HQC) is another error function method derived from information theory, distinguished by its inclusion of the ln(ln(n)) term, where n is the sample size. Unlike the Akaike Information Criterion (AIC), which focuses on minimizing the information loss with less emphasis on the sample size, HQC introduces a balance between model complexity and the consistency of model selection across different sample sizes. This ln (ln(n)) term makes HQC more conservative than AIC in terms of penalizing the number of parameters, especially as the sample size increases. Consequently, HQC is valued for its high level of consistency in model selection, particularly in scenarios where the goal is to avoid overfitting while considering the impact of sample size on model reliability and validity. This makes HQC a preferable choice in statistical evaluations that demand a more nuanced approach to model selection, particularly in the context of larger datasets [10];

$$HQC = n \times ln \frac{RSS}{n} + 2 \times p \times ln(\ln n)$$
 (Eqn. 26)

Another is MPSD. Marquardt's Percent Standard Deviation (MPSD) serves as another crucial metric in the realm of statistical model evaluation. Unique in its approach, MPSD is an error function that aligns with the distribution of the geometric mean error, enabling it to incorporate a penalty for the model based on the number of parameters. This characteristic is particularly valuable for assessing model performance in a manner that accounts for the complexity introduced by additional parameters.

By penalizing models for having a higher number of parameters, MPSD aids in mitigating the risk of overfitting, ensuring that the selected model does not merely capture the noise or the specific intricacies of the dataset at hand. Consequently, MPSD fosters the selection of models that maintain a balance between accuracy and simplicity, promoting generalizability and robustness in predictive analytics. This focus on penalizing parameter count while evaluating model error through the geometric mean makes MPSD a distinctive and useful tool in statistical analysis and model selection processes (Eqn. 27).

$$MPSD = 100 \sqrt{\frac{1}{n-p} \sum_{i=1}^{n} \left(\frac{Ob_i - Pd_i}{Ob_i}\right)^2}$$
 (Eqn. 27)

where n is the number of experimental data, p is the number of parameters, Ob_i is the experimental data, and Pd_i is the value predicted by the model.

RESULTS AND DISCUSSION

Effect of bed depth on breakthrough curve

The analysis of breakthrough curves from column experiments at varying bed depths reveals a distinct pattern; as the bed depth increases from 1 cm to 1.5 cm, and further to 2 cm, there is a noticeable extension in both breakthrough and exhaustion times. Specifically, the breakthrough times augmented from 0.216 hours to 0.383 hours, and subsequently to 0.686 hours, while exhaustion times escalated from 0.369 hours to 0.561 hours, and then to 0.686 hours, as demonstrated in Fig. 1 and detailed in Table 1. In parallel, both the breakthrough and exhaustion volumes showcased an upward trend in line with the increased bed depths. Moreover, a notable change was observed in the shape of the breakthrough curves; with the increment in bed depth, the slopes of these curves became markedly gentler. This shift indicates the development of a broader mass transfer zone, which widened from 0.618 to 0.771, and eventually to 0.932. These observations align with findings from previous studies, which have similarly documented the impact of bed depth on the dynamics of column adsorption processes [3,11–15].

Generally speaking, increasing the bed depths increases the MTZ. For instance, a study that explored the use of a biocomposite adsorbent derived from eggshells and sugarcane bagasse for removing Pb(II) ions found that increasing the bed depth from 4 to 12 cm extended the column's lifespan and increased the MTZ, indicating a more efficient adsorption process. The study also observed that a higher bed depth resulted in a minor portion of the bed remaining unused, suggesting an optimal range for bed depth to maximize efficiency and adsorbent usage [16]. In a fixed-bed study on the adsorption of phosphate by dolochar, increasing the column bed depths from 1.5 to 3 and 4.5 cm increases the MTZ from 1.08 to 1.99 and 2.50, respectively [3].

Another study for the adsorption of heavy metal ions using green macroalga highlighted that the MTZ and bed depth relationship is not linear, with the MTZ continuously expanding along the column length. This indicates that both advection and dispersion processes govern the sorbate transport, and the MTZ's expansion suggests an increase in the efficiency of the adsorption process with bed depth [17]. Finally, a study by Yinhai He et al. on the simultaneous removal of phosphate and ammonium using modified zeolite in a fixed-bed column found that the adsorption capacity increased with bed depth.

Table 1. Experimental parameters of breakthrough curves for BSA adsorption to PKC at different bed depths and concentrations of BSA.

L	Mass	Q	C_0		t_b	te (95%)	V_b	V_e	MTZ	t_z	U_z	EBCT	U_r	q_{total}	t_{e}	q_e	BSA_{total}	R	t_s	t_u	T_t	L_b	LUB
(cm)	g	L/h	mg/L	mg/h	h	h	L	L	cm	h	cm/h	h	g/L	mg	(h)	mg/g	mg	%	h	h	h	cm	cm
1	1.05	0.09	500	45.00	0.216	0.566	0.019	0.051	0.618	0.350	1.767	0.022	54.01	16.605	0.369	15.814	25.470	65.194	0.391	0.270	0.807	0.360	0.448
1.5	1.45	0.09	500	45.00	0.383	0.788	0.034	0.051	0.771	0.405	1.904	0.034	42.07	25.245	0.561	17.410	35.460	71.193	0.586	0.738	0.883	1.254	0.519
2	1.98	0.09	500	45.00	0.496	0.929	0.045	0.084	0.932	0.433	2.153	0.045	44.35	30.870	0.686	15.591	41.805	73.843	0.713	0.876	1.030	1.701	0.608
1	1.05	0.09	100	9.00	0.389	0.738	0.035	0.066	0.473	0.349	1.355	0.022	4.29	4.879	0.542	4.647	6.642	73.455	8.889	0.694	0.819	0.032	0.375
1	1.05	0.09	200	18.00	0.292	0.689	0.026	0.062	0.576	0.397	1.451	0.022	4.44	8.388	0.466	7.989	12.402	67.634	6.792	0.640	0.782	0.029	0.418
1	1.05	0.09	300	27.00	0.257	0.661	0.023	0.059	0.611	0.404	1.513	0.022	5.00	11.718	0.434	11.160	17.847	65.658	5.257	0.610	0.754	0.028	0.460
1	1.05	0.09	400	36.00	0.232	0.605	0.021	0.054	0.617	0.373	1.653	0.022	2.67	14.242	0.396	13.563	21.780	65.388	9.232	0.559	0.692	0.025	0.402
1	1.05	0.09	500	45.00	0.217	0.564	0.020	0.051	0.615	0.347	1.773	0.022	3.08	16.619	0.369	15.827	25.380	65.479	6.217	0.522	0.645	0.024	0.317

The study also observed that the time for the movement of the MTZ increased with bed height, indicating that a deeper bed could provide a longer contact time and potentially more efficient adsorption [18]. These studies collectively suggest that increasing the bed depth in fixed-bed adsorption columns affects the MTZ by extending its length and improving the efficiency of the adsorption process. A deeper bed depth allows for a longer contact time between the adsorbate and adsorbent, leading to a more efficient removal of contaminants. However, the relationship between bed depth and MTZ is complex and depends on the specific system and conditions, including the type of adsorbent, adsorbate, and operational parameters.

The increase in bed depth resulted in a decrease in the equilibrium uptake capacity (q_{eq}) with the best being at 1.5 cm. However, a bed depth of higher than 1 cm causes rapid clogging of the column and a 1 cm bed depth was utilized throughout the study. The effect of increasing bed depth in fixed-bed adsorption columns on the equilibrium uptake capacity has been a subject of research in the field of water treatment and environmental engineering. Studies have explored how changes in bed depth influence the adsorption capacity, efficiency, and breakthrough curves in the removal of various contaminants. Komarabathina et al [19] explored the potential of *Liagora viscida* as a biosorbent in a packed column for lead removal. Their experiments varied bed heights between 2 to 6 cm and found that the maximum uptake of 53.90 mg/g was achieved at a bed height of 2 cm and a flow rate of 20 mL/min.

This study suggests that while increasing bed depth can enhance adsorption capacity, there exists an optimal bed height beyond which further increases do not necessarily lead to higher q_{eq} . In a study by Karami et al.[20], the adsorption potentials of an iron-based metal-organic framework (Fe-BTC) for methyl orange removal were examined through both batch and fixed-bed column studies. The research showed that at bed depths of 0.75 and 1.5 cm, the breakthrough times were 20.0 and 46.2 h, respectively, with maximum adsorption capacities of 20.2 and 21.6 mg/g. This indicates that while increasing the bed depth did result in longer breakthrough times, the increase in maximum adsorption capacity was marginal, suggesting a diminishing return on adsorbent uptake with increased bed depth [20]. In a fixed-bed study on the adsorption of phosphate by dolochar, increasing the column bed depths from 1.5 to 3 and to 4.5 cm did not increase the q_{eq} values [3]. A similar result was also reported for the removal of phosphate from aqueous solutions by a mixture of ground burnt patties and red soil [21].

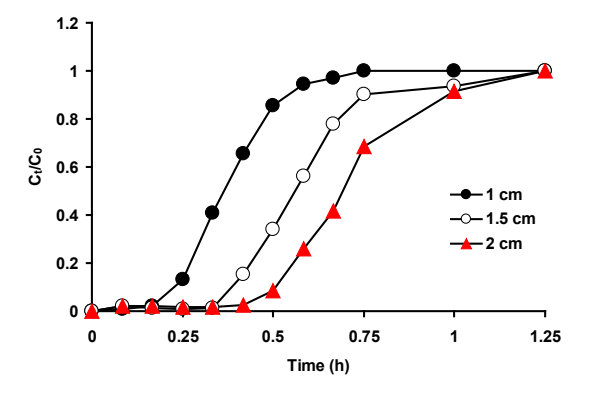


Fig. 1. Experimental breakthrough curves of BSA adsorption to PKC at different bed depths.

Effect of initial BSA concentrations on breakthrough curve

Exploring the impact of varying initial BSA concentrations on the adsorption dynamics, initial BSA concentrations were adjusted within a range of 100 to 500 µg/mL, while keeping the flow rate and bed height constant at 1 mL/min and 1 cm, respectively. The resultant breakthrough curves, depicted in Fig. 2, clearly demonstrate an inverse relationship between the initial BSA concentration and both the breakthrough and exhaustion times (and volumes). Specifically, at higher BSA concentrations in the influent, the breakthrough curves were observed to be more pronounced and steeper, leading to an earlier onset of breakthrough compared to scenarios with lower influent concentrations, which exhibited more gradual breakthrough curves and delayed bed saturation alongside a shorter mass transfer zone (MTZ). This phenomenon can be attributed to the role of intra-particle diffusion as the governing mechanism in the adsorption process, which is inherently dependent on concentration.

Consequently, variations in the concentration gradient directly influence both the breakthrough timing and the rate of saturation. Higher initial concentrations of BSA introduce a greater driving force, effectively countering the resistance to mass transfer and thus precipitating a quicker exhaustion of the adsorbent bed. Conversely, lower concentrations of the adsorbate lead to slower diffusion rates, attributed to a reduced mass transfer coefficient, thereby extending the exhaustion timeframe of the column [21,22].

The effect of increasing concentrations of adsorbate on the Mass Transfer Zone (MTZ) in fixed-bed adsorption has been the focus of various studies, aiming to understand how this parameter influences the efficiency and dynamics of adsorption processes. In one study, Dou et al. [23] explored HCl removal using a self-prepared sorbent in a fixed-bed reactor, focusing on the breakthrough curves and MTZ at high temperatures. Their study revealed that the MTZ is significantly influenced by initial concentration, flow velocity, and chemical reaction parameters.

The breakthrough time was found to be proportional to the depth of the fixed-bed, indicating that higher initial concentrations of adsorbate could potentially lead to a quicker saturation of the adsorbent near the inlet, thus expanding the MTZ. In another study, Ibrahim et al. investigated the adsorption of sulfur dioxide (SO2) on NiO supported activated carbon in a fixed-bed reactor. Their study found that increasing the gas flow rate and bed height influenced the characteristics of the MTZ, with higher adsorbate concentrations leading to quicker breakthrough times and an expanded MTZ, which is similarly observed in this study [24]. Lastly, Ghorbani et al [25] conducted dynamic modeling and simulation of the fixed-bed adsorption process, focusing on the breakthrough curve parameters for sulfur compound removal from fuel. Their findings also showed that higher inlet concentrations of adsorbate result in a more utilized overall bed capacity and influence the height and behavior of the MTZ.

These studies collectively indicate that increasing concentrations of adsorbate in fixed-bed adsorption processes significantly impact the MTZ, affecting both the efficiency and dynamics of adsorption. Higher adsorbate concentrations tend to expand the MTZ, influencing breakthrough times and adsorption capacity. Understanding these effects is crucial for the design and optimization of fixed-bed adsorption systems, ensuring effective contaminant removal and efficient use of adsorbent materials. Conversely, as the initial BSA concentration was escalated from

100 to 500 mg/L, there was a notable increase in the uptake capacity of PKC, rising from 7.99 to 15.827 mg/g, respectively.

This enhancement in uptake capacity can be ascribed to the augmented driving force for diffusion alongside an increase in the adsorbate loading rate, which is a direct consequence of the elevated initial BSA concentration. This observation aligns with findings from previous studies, such as a fixed-bed analysis on phosphate adsorption using dolochar. In that study, elevating the inlet phosphate concentrations from 5 to 15 mg/L led to an increase in the equilibrium uptake values (q_{eq}) from 2.87 to 6.13 mg/g, underscoring the influence of initial concentration on the adsorption capacity in fixed-bed columns [3]. Owing to the uptake capacity, 500 mg/L initial BSA concentration was considered in this for further experimentations.

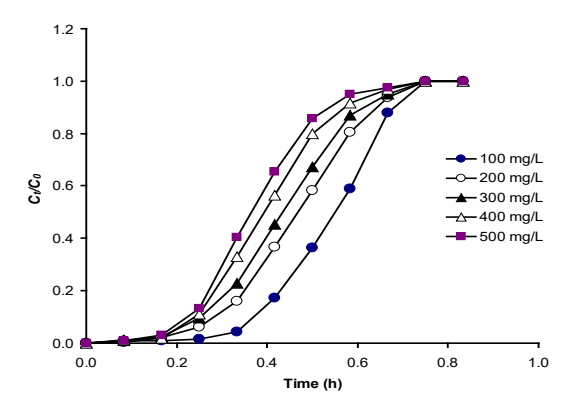


Fig. 2. Experimental breakthrough curves of BSA adsorption to PKC at different concentrations.

Best model according to error function analysis

Both MDR and the Thomas model are two-parameter models, and the power of penalty-imposing error functions below would be the same. The three curves for the bed depths data (1, 1.5 and 2 cm) were subjected to error function analysis and the results were averaged [26]. An overwhelming majority of the error function analyses show that the MDR model performs better than the Thomas model with the lowest RMSE, AICc, BIC, HQC and AdjR2 value closest to unity. The error functions MPSD, AF and BF values on the other hand indicate that the Thomas model was the best (**Table 2**). Based on this, MDR was chosen as the best model.

Table 2. Averaged error functions for three different bed depth curves.

	MDR	Thomas
MPSD	2.352	2.238
RMSE	0.019	0.023
adR ²	0.998	0.996
AICc	-85.016	-80.131
BIC	-93.046	-88.162
HQC	-94.375	-89.491
BF	0.431	0.934
AF	3.686	1.493

Application of the Thomas model

The breakthrough data obtained from BSA adsorption under various experimental setups were analyzed using the Thomas model through a nonlinear regression technique. The resultant predicted and experimental breakthrough curves are presented in **Figs. 3** to **4**, with the associated model parameters detailed in **Table 3**. An examination of the data in **Table 3** reveals that the Thomas model constant *A* exhibits an increase with heightened bed depths, yet shows a decrease as the influent BSA concentration rises. On the contrary, constant *B* displays a varied

trend compared to A. A similar pattern in the influence of inlet concentrations on these constants is documented in **Table 4**. With regards to the parameters K_{Th} and q_{Th} , an observation from **Table 3** indicates a decline in both parameters with an increment in bed depths. This trend can likely be attributed to an elevated mass transfer resistance occurring as a result of the increased bed depth within the columns, affecting the overall efficiency of the adsorption process. The effect of inlet concentrations showed that the K_{Th} parameter decreased whilst the q_{Th} parameter was increased and the reasons for this increased has been discussed above.

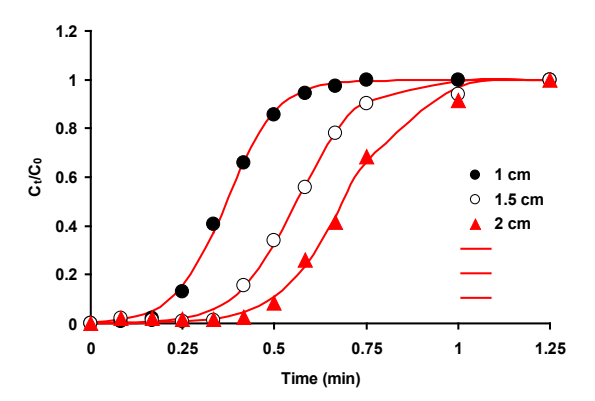


Fig. 3. Experimental and predicted breakthrough curves of BSA adsorption to PKC at different bed depths as modelled using the Thomas model (C_0 =500 mg/L and Q = 1.5 mL/min).

Table 3. Estimated parameters of the Thomas model for BSA adsorption to PKC at different bed depths (C_0 =500 mg L^{-1} and Q = 1.5 mL min⁻¹).

			C_0		Α	В	K_{Th}	q_{Th}
L (cn	n)	Q(L/h)	(mg/L)	m (g)	Thomas	Thomas	(L/h/mg)	(mg/g)
1.00)	0.09	500	1.05	5.29	14.34	0.03	15.82
1.50)	0.09	500	1.45	6.81	12.12	0.02	17.43
2.00)	0.09	500	1.98	7.70	11.17	0.02	15.67

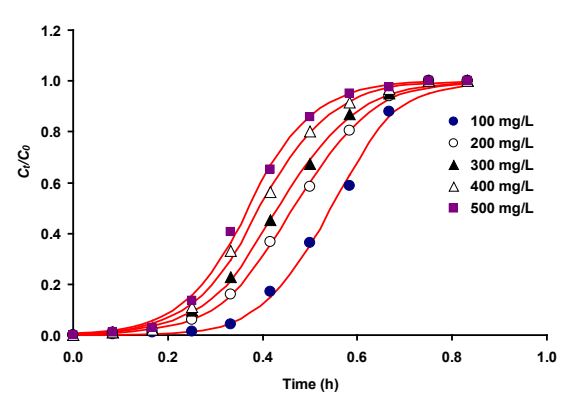


Fig. 4. Experimental and predicted breakthrough curves of BSA adsorption to PKC at various BSA concentrations as modelled using the Thomas model (L = 1 cm and Q = 1.5 mL/min).

Table 4. Estimated parameters of the MDR model for BSA adsorption to PKC at various BSA concentrations as modelled using the Thomas model (L = 1 cm and Q = 1.5 mL/min).

L	Q	C_0		A	B	K_{Th}	q_{Th}
(cm)	(L/h)	(mg/L)	m (g)	Thomas	Thomas	(L/h/mg)	(mg/g)
1	0.09	100	1.05	7.75	14.294	0.143	4.65
1	0.09	200	1.05	5.873	12.58	0.063	8.0
1	0.09	300	1.05	5.368	12.346	0.041	11.18
1	0.09	400	1.05	5.251	13.259	0.033	13.58
1	0.09	500	1.05	5.2	14.076	0.028	15.83

Application of Modified dose response model

The breakthrough data for BSA adsorption under various experimental conditions were analyzed using the Modified Dose Response (MDR) model through a nonlinear regression method. The resulting experimental and predicted breakthrough curves are depicted in Figs. 5 and 6, with the corresponding model parameters detailed in Tables 5 and 6. An analysis of the data reveals that the parameter b of the MDR model tends to increase with greater bed depths but decreases as the inlet BSA concentration rises. Conversely, the parameter a shows an upward trend with both increasing bed depths and higher BSA concentrations. This trend is reflective of the dynamics observed in a similar fixed-bed adsorption study of phosphate using dolochar, where deeper bed depths led to an increase in both a and b parameters of the MDR model. However, a higher inlet concentration resulted in a decrease in the b parameter, while the effect on the a parameter varied, indicating the complex interaction between bed depth, influent concentration, and adsorption capacity in fixed-bed systems [3].

The maximum solid phase concentration of the solute (q_m) exhibited a decrease with increasing bed depth and flow rate, but it showed an increase with higher initial BSA concentrations. This trend can be attributed to the influence of mass transfer resistance, the inadequacy of contact between adsorbate and adsorbent, and a diminished driving force for adsorption under certain conditions. Similar observations were noted in a fixedbed study focusing on phosphate adsorption using dolochar, where an increase in bed depths led to a reduction in the q_m value as per the MDR model [3]. Moreover, a comparison reveals that the q_m values derived from the MDR model closely align with the qe values obtained from experimental measurements across all tested conditions. This consistency underscores the MDR model's suitability for accurately predicting the breakthrough curves in adsorption processes, thereby validating its applicability and effectiveness in modeling adsorption dynamics under various operational parameters.

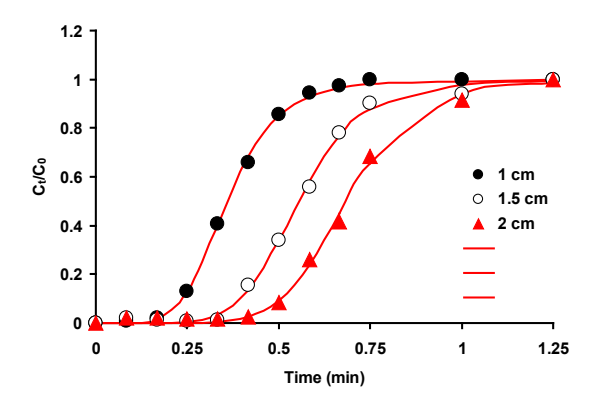


Fig. 5. Experimental and predicted breakthrough curves of BSA adsorption to PKC at different bed depths as modelled using the MDR model (C_0 =500 mg/L and Q = 1.5 mL/min).

Table 5. Estimated parameters of the MDR model for BSA adsorption to PKC at different bed depths (C_0 =500 mg/L and Q = 1.5 mL/min).

L	Q (L	C0		a (MDR	b (MDR	q_m (mg
(cm)	h ⁻¹)	(mg/L)	m (g)	constant)	constant)	g-1)
1	0.09	500	1.05	5.307	0.032	15.24
1.5	0.09	500	1.45	6.527	0.05	17.24
2	0.09	500	1.98	7.19	0.062	15.66

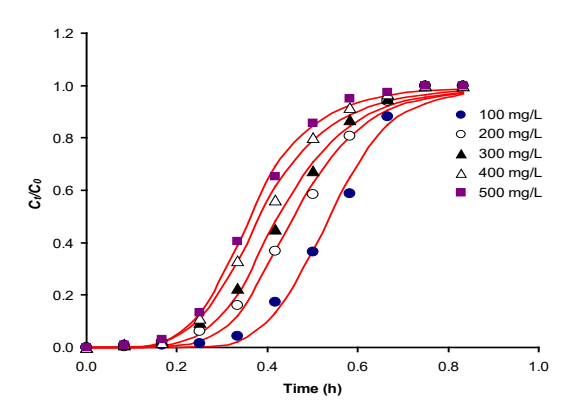


Fig. 6. Experimental and predicted breakthrough curves of BSA adsorption to PKC at various BSA concentrations as modelled using the MDR model (L = 1 cm and Q = 1.5 mL/min).

Table 6. Estimated parameters of the MDR model for BSA adsorption to PKC at various BSA concentrations as modelled using the MDR model (L = 1 cm and Q = 1.5 mL/min).

L (cm)						
(height		C_0		a (MDR	b (MDR	
of bed)	Q (L h-1)	(mg/L)	m (g)	constant)	constant)	$q_m (\text{mg g}^{-1})$
1	0.09	100	1	7.896	0.048	4.8
1	0.09	200	1	5.994	0.041	8.2
1	0.09	300	1	5.446	0.038	11.4
1	0.09	400	1	4.935	0.034	13.6
1	0.09	500	1	5.231	0.032	16

CONCLUSION

The analysis demonstrates that increasing the bed depth in adsorption column experiments from 1 cm to 2 cm significantly extends both breakthrough and exhaustion times, indicating improved adsorption efficiency with deeper beds, albeit with a noted increase in column clogging at depths greater than 1 cm. Additionally, higher initial BSA concentrations lead to quicker breakthroughs due to a stronger driving force overcoming mass transfer resistance. The Modified Dose Response (MDR) model outperformed the Thomas model in accurately predicting breakthrough curves across different bed depths and BSA concentrations, as determined by error function analysis. However, the Thomas model still provided valuable insights into the dynamics of adsorption, particularly highlighting the interplay between bed depth, influent concentration, and model constants. Ultimately, the study underscores the complexity of optimizing adsorption processes in agrisorption, balancing between bed depth, adsorbate concentration, and the appropriate modeling approach to accurately predict system performance. The results indicate the high possibility of using PKC as an adsorbent for protein-rich agriculture, poultry and farm animal waste to improve the nutritional content of PKC.

ABBREVIATION

Q is the volumetric flow	rate (L/h)
--------------------------	------------

 C_0 Initial concentration of BSA (mg/L)

 t_b Time breakthrough (h), effluent BSA concentration < 1 mg/L Time exhaustion (h), 80% of influent BSA appears in the

t_e effluent.

Volume breakthrough (L), effluent BSA concentration < 1

 V_b mg/L

Volume exhaustion (L), 80% of influent BSA appears in the

 V_e effluent $V_e = Qt_e$ volume of solution treated at exhaustion (L)

MTZ mass transfer zone (cm),

time required for the MTZ to move the length of its own height up/down the column (h).

- U_z the rate of movement of MTZ (cm/h)
- EBCT empty bed contact time (h)
- U_r adsorbent usage rate (g/L)
- q_{total} total BSA adsorbed (mg)
- q_{eq} equilibrium BSA uptake capacity of the column (mg/g)
- D_{total} total amount of BSA entering the column (mg)
- R percentage removal of BSA (%)
- stoichiometric time for unsymmetrical break time at which $C_r/C_0 = 0.5$ and for a symmetrical breakthrough curve (h) time at which the effluent concentration reaches its maximum
- t_u permissible limit (h)
- L_b the length of bed used up to the breakthrough time (cm)
- LUB length of unused bed (cm)

REFERENCES

- Onn HW. Are we ready to upgrade palm kernel cake? [Internet]. NST Online. 2022 [cited 2024 Feb 7]. Available from: https://www.nst.com.my/opinion/columnists/2022/06/804991/are-we-ready-upgrade-palm-kernel-cake
- Oladipo AA, Gazi M. Fixed-bed column sorption of borate onto pomegranate seed powder-PVA beads: a response surface methodology approach. Toxicol Environ Chem. 2014 Jul 3;96(6):837–48.
- Rout PR, Bhunia P, Dash RR. Evaluation of kinetic and statistical models for predicting breakthrough curves of phosphate removal using dolochar-packed columns. J Water Process Eng. 2017 Jun 1:17:168–80.
- Afroze S, Sen TK, Ang HM. Adsorption performance of continuous fixed bed column for the removal of methylene blue (MB) dye using *Eucalyptus sheathiana* bark biomass. Res Chem Intermed. 2016 Mar 1:42(3):2343–64.
- Chu KH. Fixed bed sorption: setting the record straight on the Bohart-Adams and Thomas models. J Hazard Mater. 2010 May 15:177(1-3):1006-12.
- Lee CG, Kim JH, Kang JK, Kim SB, Park SJ, Lee SH, et al. Comparative analysis of fixed-bed sorption models using phosphate breakthrough curves in slag filter media. Desalination Water Treat. 2015 Aug 14:55(7):1795–805.
- 2015 Aug 14;55(7):1795–805.
 7. Wayman M, Tseng MC. Inhibition-threshold substrate concentrations. Biotechnol Bioeng. 1976;18(3):383–7.
- Głuszcz P, Petera J, Ledakowicz S. Mathematical modeling of the integrated process of mercury bioremediation in the industrial bioreactor. Bioprocess Biosyst Eng. 2011;34(3):275–85.
- Kass RE, Raftery AE. Bayes Factors. J Am Stat Assoc. 1995 Jun 1:90(430):773–95.
- Burnham KP, Anderson DR. Model Selection and Multimodel Inference: A Practical Information-Theoretic Approach. Springer Science & Business Media; 2002. 528 p.
- Ghosh A, Chakrabarti S, Ghosh UC. Fixed-bed column performance of Mn-incorporated iron(III) oxide nanoparticle agglomerates on As(III) removal from the spiked groundwater in lab bench scale. Chem Eng J. 2014;248:18–26.
- Rout PR, Bhunia P, Dash RR. Modeling isotherms, kinetics and understanding the mechanism of phosphate adsorption onto a solid waste: Ground burnt patties. J Environ Chem Eng. 2014;3(2):1331– 42.
- Rout PR, Bhunia P, Dash RR. A mechanistic approach to evaluate the effectiveness of red soil as a natural adsorbent for phosphate removal from wastewater. Desalination Water Treat. 2015 Apr 10;54(2):358–73.
- Mani SK, Bhandari R. Efficient Fluoride Removal by a Fixed-Bed Column of Self-Assembled Zr(IV)-, Fe(III)-, Cu(II)-Complexed Polyvinyl Alcohol Hydrogel Beads. ACS Omega. 2022 May 3:7(17):15048–63.
- Cheng Y, Yang J, Shen J, Yan P, Liu S, Kang J, et al. Preparation of P-doped biochar and its high-efficient removal of sulfamethoxazole from water: Adsorption mechanism, fixed-bed column and DFT study. Chem Eng J. 2023 Jul 15;468:143748.
- Harripersadth C, Musonge P. The Dynamic Behaviour of a Binary Adsorbent in a Fixed Bed Column for the Removal of Pb2+ Ions from Contaminated Water Bodies. Sustainability. 2022 Jan;14(13):7662.
- Apiratikul R. Application of analytical solution of advectiondispersion-reaction model to predict the breakthrough curve and

- mass transfer zone for the biosorption of heavy metal ion in a fixed bed column. Process Saf Environ Prot. 2020 May 1;137:58–65.
- He Y, Lin H, Dong Y, Liu Q, Wang L. Simultaneous removal of phosphate and ammonium using salt–thermal-activated and lanthanum-doped zeolite: fixed-bed column and mechanism study. Desalination Water Treat. 2016 Dec 1;57(56):27279–93.
- Komarabathina S, King P, Pujari M. Breakthrough Studies of the Adsorption of Lead from Synthetic Solution using Liagora Viscida in a Fixed Bed Column. Environ Prog Sustain Energy. 2021 Feb 8:40.
- Karami A, Sabouni R, Al-Sayah M, Aidan A. Adsorption potentials
 of iron-based metal-organic framework for methyl orange removal:
 batch and fixed-bed column studies. Int J Environ Sci Technol.
 2021 Jan 4:18.
- 21. Rout P, Bhunia P, Dash R. Modelling and packed bed column studies on adsorptive removal of phosphate from aqueous solutions by a mixture of ground burnt patties and red soil. Adv Environ Res. 2014 Sep 1;3:231–51.
- Nur T, Johir MAH, Loganathan P, Nguyen T, Vigneswaran S, Kandasamy J. Phosphate removal from water using an iron oxide impregnated strong base anion exchange resin. J Ind Eng Chem. 2014 Jul 25:20(4):1301–7.
- Dou B, Gao J, Back S, Sha X. High-Temperature HCl Removal with Sorbents in a Fixed-Bed Reactor. Energy Fuels - ENERG FUEL. 2003 Jul 1;17.
- 24. Ibrahim NK, Raouf SR, Nasir ZA. Removal of SO2 over Modified ActivatedCarbon in Fixed Bed Reactor: II.Effect ofProcess Variables on the Characteristics of Mass Transfer Zone. Eng Technol J [Internet]. 2014 [cited 2024 Feb 12];32(7 Part (A) Engineering). Available from: https://www.iasj.net/iasj/article/99914
- Ghorbani A, Karimzadeh R, Mofarahi M. Mathematical Modeling of Fixed Bed Adsorption: Influence of Main Parameters on Breakthrough Curve. J Chem Pet Eng. 2018;52(2):135–43.
- Hardt M, Schraknepper D, Bergs T. Investigations on the Application of the Downhill-Simplex-Algorithm to the Inverse Determination of Material Model Parameters for FE-Machining Simulations. Simul Model Pract Theory. 2021 Feb 1;107:102214.